Electronic Supplementary Material (ESI) for Chemical Communications.

Supporting Information

Cascaded Bandgap Design for Highly Efficient Electron Transport Layer-Free Perovskite Solar Cells

Liguo Gao[a,*], Cai Xu[a], Yingjie Su[a], Anmin Liu[a], Tingli Ma[b,c]

a State Key Laboratory of Fine Chemicals, Dalian University of Technology, Dalian 116023, China.

b College of Materials and Chemistry, China Jiliang University, Hangzhou, 310018, China.

c Graduate School of Life Science and Systems Engineering, Kyushu Institute of Technology, Kitakyushu, Fukuoka 808-0196, Japan.

Corresponding Author

*Liguo Gao

E-mail: liguo.gao@dlut.edu.cn; ORCID: 0000-0002-5390-3663.

Experimental Section

Materials

Indium-tin-oxide (ITO) was purchased from Yingkou OPV Tech New Energy Co., Ltd. BAI (99.5%), CsI (99.9%), $PbBr_2$ (99.9%), MABr (99.5%), FAI (99.5%) were purchased from Xi'an Polymer Light Technology Corp. BACl (99.8%) was purchased from Macklin. Dimethyl sulfoxide (DMSO, hybridoma, 99.7%), N, N-dimethylformamide (DMF, for HPLC, 99.9%), Tin(II) chloride dihydrate ($SnCl_2 \cdot 2H_2O$, 98%), and Chlorobenzene (99.9%) were purchased from Sigma-Aldrich. Tin(IV) oxide (SnO_2, hydrosol, 15%wt) was purchased from Afaisha (China) Chemical Co., Ltd. Anhydrous ethanol (99%) was purchased from Sinopharm

Chemical Reagent Co., Ltd. PbI_2 (99.99%) and 2,2′,7,7′-Tetrakis-[N, N-di(4-methoxyphenyl)amino]-9,9′-spirobifluorene (Spiro-OMeTAD, 99.86%) were purchased from Advanced Election Technology CO,. Ltd.

Devices fabrication

ITO substrates were cleaned by sequential ultra-sonication in detergent, deionized water, ethanol, acetone, and ethanol for 30 min each. The tri-cation perovskite material $Cs_{0.05}(FA_{0.83}MA_{0.17})_{0.95}Pb(I_{0.83}Br_{0.17})_3$ was composed of FAI (1.19 M), PbI_2 (1.31 M), MABr (0.21 M), $PbBr_2$ (0.21 M), and CsI (0.07 M), which were dissolved in a mixed solvent with a volume ratio of DMSO:DMF = 1:4.

For the traditional structure devices with ETL, the SnO_2 was used as ETL. The SnO_2 hydrosol was diluted by deionized water and dropped onto the cleaned ITO glass treated by ultraviolet ozone (UVO) for 25 min, then spin-coated at 2000 rpm 30 s. The SnO_2 film on ITO glass was sequentially annealed at 150 °C for 40 min. Subsequently, 0.1M $SnCl_2$ solution was dropped onto the ITO/SnO_2 substrate and spin-coated at 6000 rpm 30 s. Then, it was annealed at 100 °C for 10 min and 180 °C for 1 h. After 15 min UVO treatment, the perovskite precursor was spin-coated onto the treated substrate. The perovskite precursors are spin-coated in two steps (1000 rpm for 10 s and 5000 rpm for 30 s). During the 15th second of the main step, 150 μL chlorobenzene was dropped onto the perovskite surface, followed by annealing at 100 °C for 75 min. Spiro-OMeTAD was utilized as the HTLs by spin-coated at 3500 rpm for 30 s. The solution of the HTLs was prepared by adding 72.3 mg Spiro-OMeTAD, 28.8 μL 4-tert-butylpyridine (tBP), 17.5 μL of a stock solution of 520 $mg \cdot mL^{-1}$ lithium bis-(trifluoromethyl sulphonyl) imide (Li-TFSI), and 20.0 μL of a stock solution of 300 $mg \cdot mL^{-1}$ tris(1-(pyridin-2-yl)-1H-pyrazol) cobalt(iii) tris(hexafluorophosphate) (FK102) in acetonitrile to 1 mL chlorobenzene. Finally, 80 nm of gold was deposited by thermal evaporation using a shadow mask to pattern the electrodes.

For the ETL-free PSCs based on CPVK, the clean ITO was treated by UVO for 25 min. The perovskite precursors are spin-coated in two steps (1000 rpm for 10 s and

5000 rpm for 30 s). During the 15th second of the main step, 150 μL chlorobenzene was dropped onto the perovskite surface, followed by annealing at 100 °C for 75 min. The HTL and counter electrode were fabricated the same as the traditional structure devices.

For the GHJP ETL-free devices, BAI (0.46 g/L) was dissolved in DMSO. Firstly, the cleaned ITO substrates were treated by UVO for 25 min. Then, BAI solution was dropped on it and spin-coated for 10 s at 2250 rpm and 30 s at 5000 rpm. During the 5th second, the perovskite precursor was dropped in the center of BAI solution. During the high-speed stage, 150 μL chlorobenzene, utilized as an antisolvent, was dropped onto the perovskite surface at the 25th second, followed by annealing at 100 °C for 75 min. The HTL and counter electrode were fabricated the same as the traditional structure devices.

Characterizations

Time of flight secondary ion mass spectrometry (ToF-SIMS) depth profiles was measured using Bruker extreme MALDI-TOF to determine devices structure. The properties of perovskite films were characterized by X-ray photoelectron spectroscopy (XPS) was conducted on a Thermo Scientific, ESCLAB 250Xi, USA. The femtosecond transient absorption (fs-TA) measurement was performed by an Ultrafast System HELIOS spectrometer with a laser source of the Coherent Legend regenerative amplifier (35 fs, 1 Hz, 800 nm) seeded by a Coherent Vitesse oscillator (30 fs, 80 MHz). A ~ 10 μJ portion of the fundamental 800 nm laser was directed into a CaF_2 crystal to produce the probe pulses (350–800 nm). The structure properties of perovskite films were performed by X-ray diffraction (XRD-7000 S, Shimadzu) from 5° to 60°. The SEM (FEI Nova Nano SEM 450) was applied to observe the morphology of the perovskite. The energy level positions of perovskite materials were tested by Ultraviolet photoelectron spectroscopy (UPS), He I (hν = 21.2 eV) was used as the emission source and all measurements were calibrated with Au. The Nyquist chart tests were performed using an electrochemical workstation (Zennium Zahner, Germany) at a 0.6 V forward bias voltages of Alternating current perturbation ranging from 100 mHz to 4 MHz meanwhile under light conditions. The incident photon to current conversion efficiency (IPCE) testing was achieved through a combination of Xenon lamps and computer-controlled monochrome (PEC-S20, Peccell). Photoluminescence (PL) spectra were obtained by using C5410 (Hamamatsu) at 517 nm excitation wavelengths. The absorbance was measured by a LAMBDA 950. The *J-V* characteristic curves were obtained by a solar simulator (Peccell-L15, Japan) under the condition of AM 1.5G (1000 W·m^{-2}, Keithley 2460, America). Transient Photocurrent (TPC), Transient Photovoltage (TPV), Intensity-modulation photovoltage spectroscopy (IMVS), Intensity-modulation photocurrent spectroscopy (IMPS), the space charge limited current (SCLC), and the linear sweep voltammetry (LSV) were also obtained using an electrochemical workstation. The SCLC was collected on ETM-only devices with a bias range of 0.001 V to 10 V.

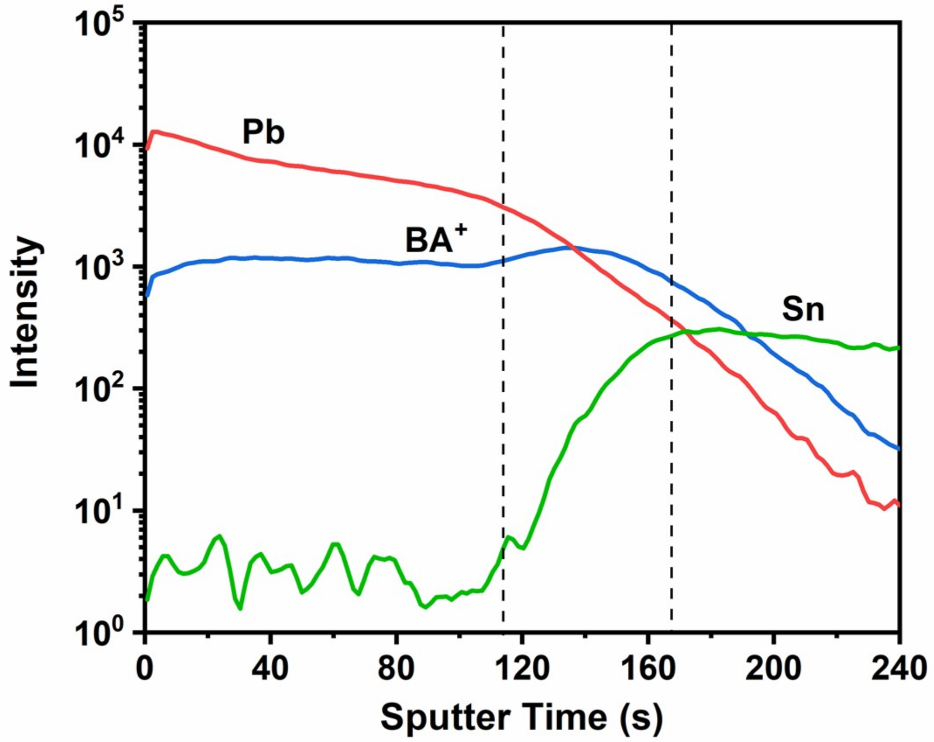

Figure S1. The ToF-SIMS depth profile of the GHJP films BA^+ (blue line) represented as BAI, Sn (green line) represented as ITO, Pb (red line) represented as perovskite). Since there is no special element in n-butylammonium iodide that can be distinguished from perovskite material, n-butylammonium chloride is used to calibrate the distribution location of large cation-assisted.

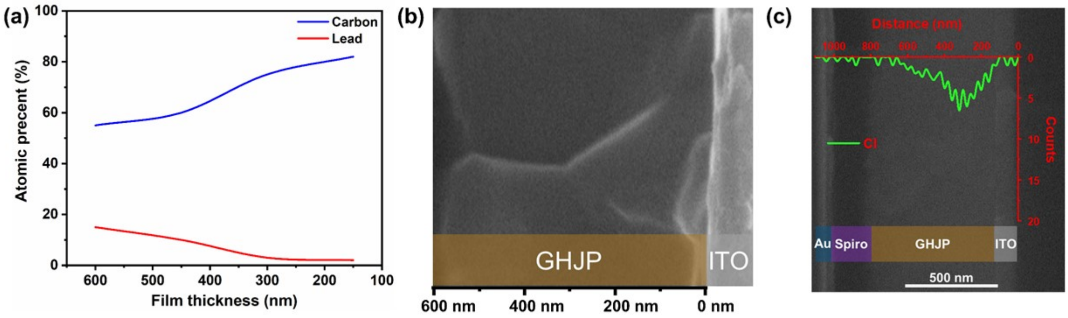

Figure S2. (a) The percentage change of carbon atom and lead atom in different depths of GHJP films (The thickness of GHJP film is about 600 nm. 600 nm to 150 nm is the thickness of perovskite left on ITO). (b) Cross-sectional SEM image of the GHJP film. (c) The Cl element profiles across the ITO/GHJP/Spiro/Au sample was determined by EDS line scan.

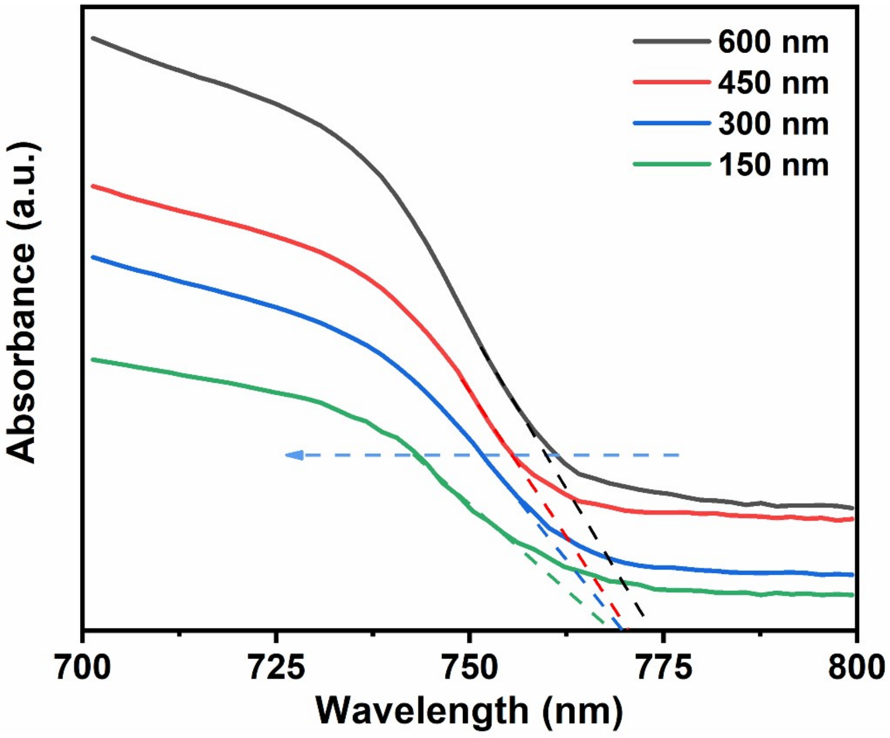

Figure S3. UV-vis absorption spectra of GHJP films in different depths (The thickness of GHJP film is about 600 nm. 600, 450, 300, and 150 nm is the thickness of perovskite left on ITO).

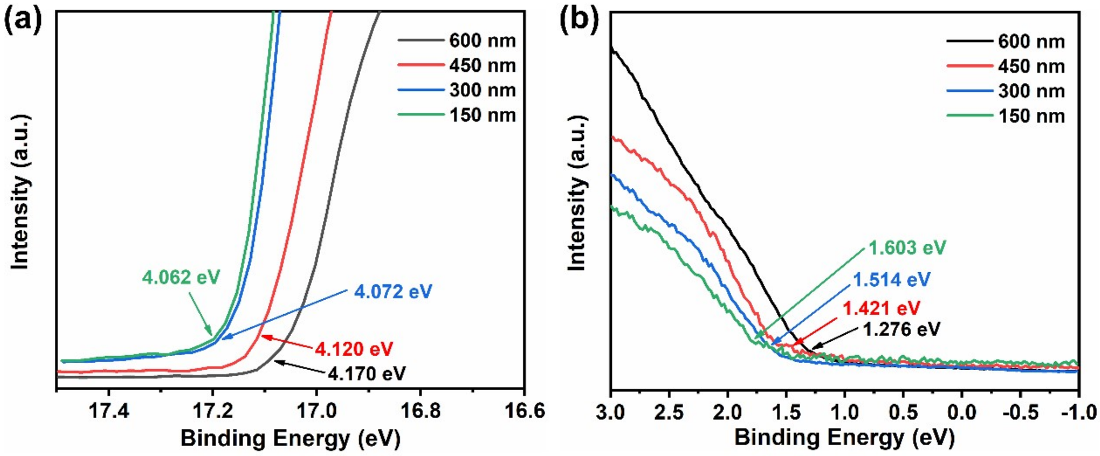

Figure S4. (a) UPS photoemission cutoff and (b) Valence band spectra of GHJP films in different depths (The thickness of GHJP film is about 600 nm. 600, 450, 300, and 150 nm is the thickness of perovskite left on ITO).

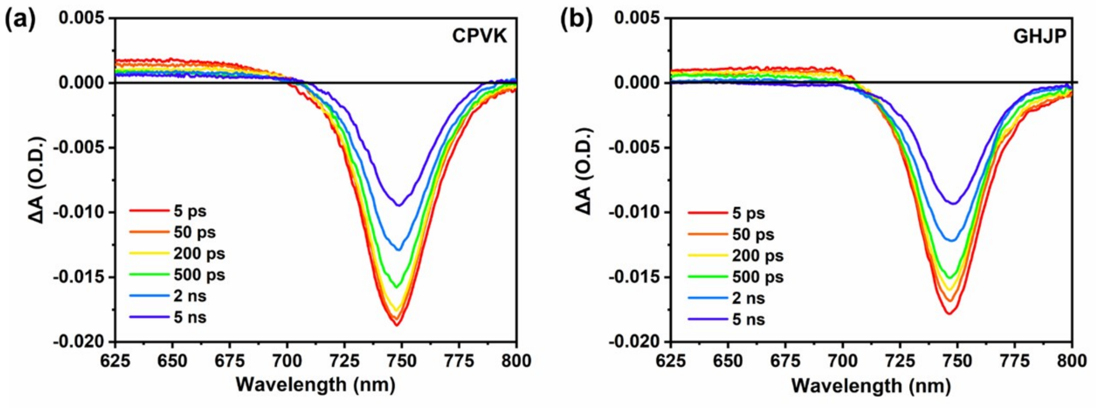

Figure S5. fs-TA spectra of perovskite films on ITO, (a) CPVK and (b) GHJP.

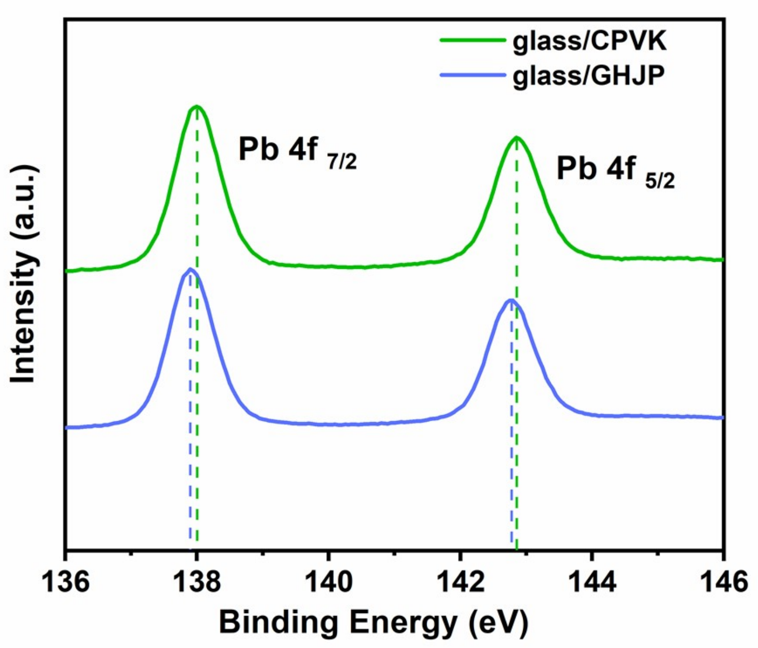

Figure S6. XPS spectra with Pb 4f core level of CPVK and GHJP films.

The SCLC curves can be divided into three different regimes, i.e., ohmic (n = 1), SCLC (n = 2), and trap-filled limited (1 < n < 2) regions according to the diverse values of the exponent n ($J \propto V_n$ relation). At a kink point where the current abruptly rises, the bias voltage is defined as the trap-filled limit voltage (V_{TFL}). From this domain, the trap density (N_t) can be calculated using the following equation:

$$V_{\mathrm{TFL}} = \frac{N_t e L^2}{2\varepsilon_0 \varepsilon_r}$$

where e is the electron charge, L is the thickness of the perovskite film, ε_0 is the vacuum permittivity, ε_r is the relative dielectric constant of the perovskite film (28.8). The N_t of the CPVK and GHJP were 3.45×10^{15} and 2.39×10^{15} cm^{-3}, respectively. The lower N_t in GHJP film is consistent with the PL quenching and enhanced film quality in the main text. At high bias voltages, the current quadratically rises with the voltage in the SCLC region (n = 2). From this regime, the charge carrier mobility can be evaluated by the Mott-Gurney law in single-carrier devices. The mobility can be calculated by the following equation:

$$J_D = \frac{9\mu\varepsilon_0\varepsilon_r V^2}{8L^3}$$

Where J_D, μ, and V are the dark current, electron mobility, and bias voltage, respectively. The μ values of the electron-only devices prepared by GHJP film (3.32×10^{-5} $\mathrm{cm}^2\cdot\mathrm{V}^{-1}\cdot\mathrm{s}^{-1}$) was higher than that prepared by CPVK film (2.63×10^{-5} $\mathrm{cm}^2\cdot\mathrm{V}^{-1}\cdot\mathrm{s}^{-1}$). LSV results showed that the electrical conductivity of GHJP film was higher than CPVK film, which implied faster charge transport and less energy loss.

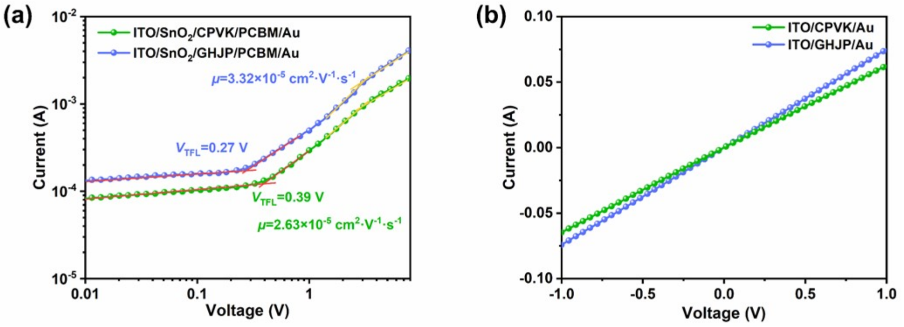

Figure S7. (a) The SCLC curves of electron-only devices. (b) The LSV characteristics of ITO/CPVK/Au and ITO/GHJP/Au structures.

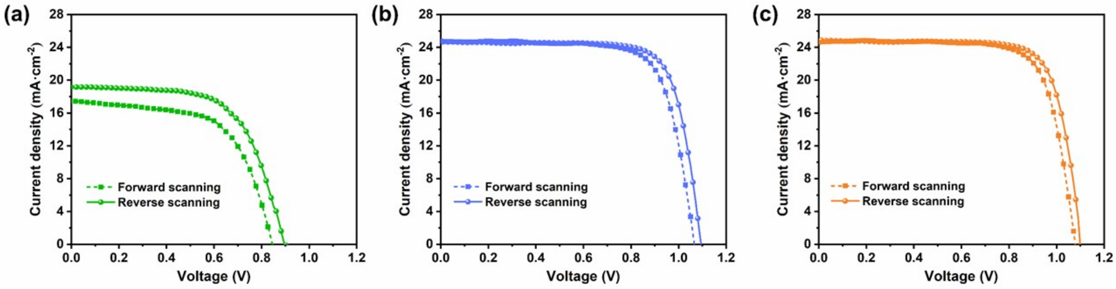

Figure S8. The forward and reverse scanning *J*-*V* curves of the champion device. (a) ETL-free PSCs based on CPVK, (b) ETL-free PSCs based on GHJP, (c) PSCs with SnO_2 as ETL.

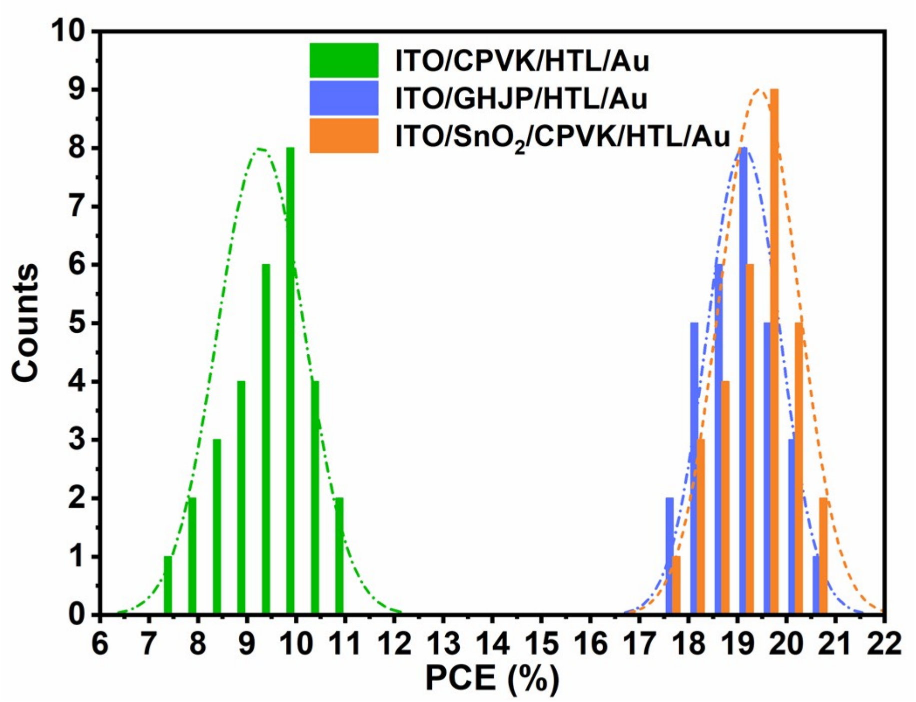

Figure S9. The histogram of efficiency distribution of 30 cells with different structures

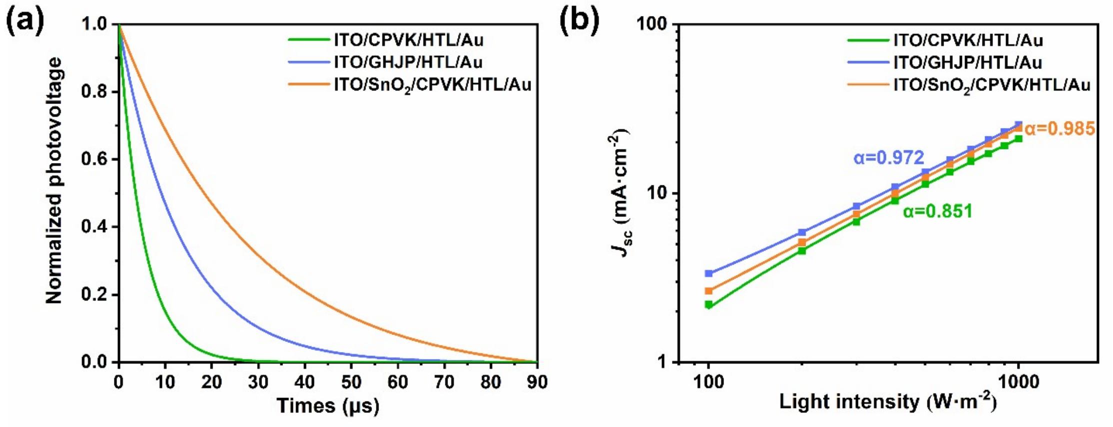

Figure S10. (a) Transient photovoltage decay curves, (b) Short-circuit current density (J_{sc}) plotted versus light intensity of the different structures.

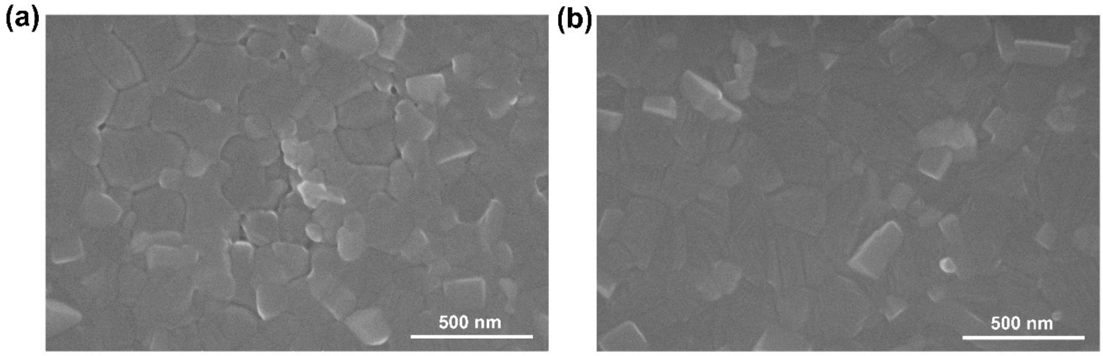

Figure S11. Top-view SEM images of (a) CPVK and (b) GHJP films.

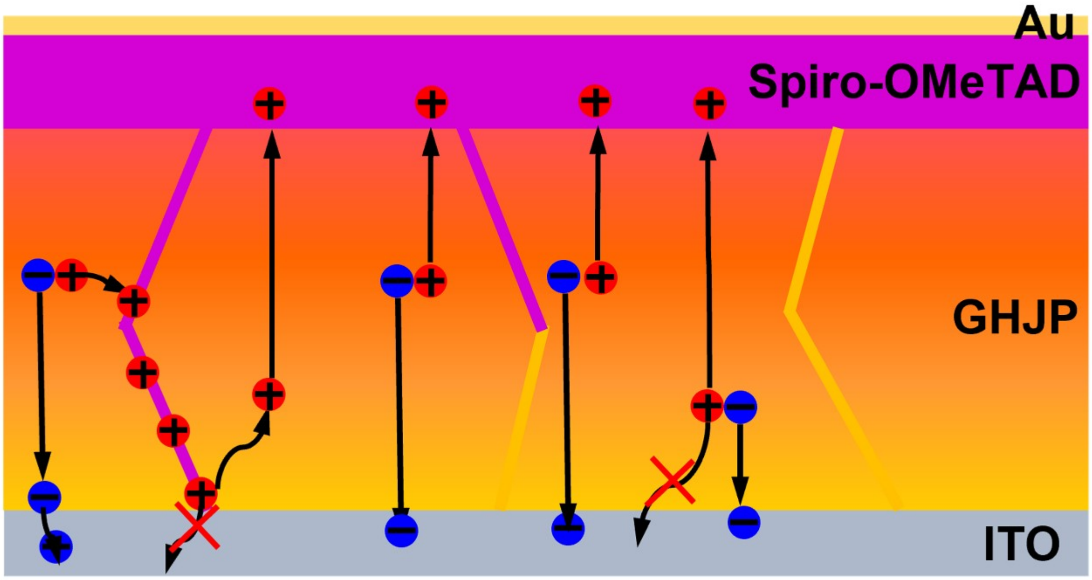

Figure S12. Charge transfer schematic diagram of ETL-free PSCs based on GHJP.

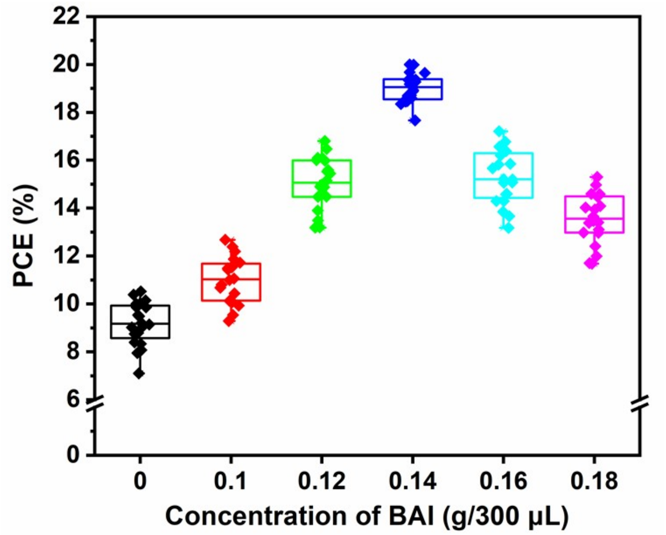

Figure S13. PCE distribution of ETL-free PSCs with different concentrations of BAI.

Table S1. *J-V* curve parameters of the champion PSCs based on different structures.

	Scan direction	V_{oc} (V)	J_{sc}(mA·cm^{-2})	FF	PCE(%)
ITO/CPVK/HTL/Au	**Forward**	**0.84**	**17.79**	**0.61**	**9.05**
	Reverse	**0.89**	**19.12**	**0.63**	**10.79**
ITO/GHJP/HTL/Au	**Forward**	**1.06**	**24.66**	**0.75**	**19.51**
	Reverse	**1.09**	**24.70**	**0.76**	**20.55**
ITO/SnO_2/CPVK/HTL/Au	**Forward**	**1.07**	**24.74**	**0.75**	**20.01**
	Reverse	**1.10**	**24.88**	**0.76**	**20.92**

Table S2. TPC, TPV, and EIS fitting results of devices based on different structures.

	TPC (μs)	**TPV (μs)**	**R_{rec} (kΩ)**
ITO/CPVK/HTL/Au	**47.2**	**5.3**	**19.9**
ITO/GHJP/HTL/Au	**33.2**	**13.3**	**50.1**
ITO/SnO_2/CPVK/HTL/Au	**26.6**	**28.2**	**49.4**